Int. J. Heat Mass Transfer. Vol. 32, No. 6, pp. 1021–1036, 1989
Printed in Great Britain

0017–9310/89 $3.00+0.00

Density stratification due to counterbuoyant flow along a vertical crystallization front

M. E. THOMPSON† and J. SZEKELY
Department of Materials Science and Engineering, Massachusetts Institute of Technology, Cambridge, MA 02139, U.S.A.

(*Received* 9 *September* 1988 *and in final form* 27 *June* 1988)

Abstract—Theoretical modelling and experimentation are used to analyze horizontal solidification of a double-diffusive, binary liquid in a confined rectangular cavity. For solutions which segregate the lighter component into the liquid, the composition and temperature gradients produced upon solidification lead to the onset of vertical counterbuoyant flow along the growing crystals. The counterflow progressively transforms the initially homogeneous liquid into a density-stratified fluid layer characterized by pronounced vertical gradients in solute concentration. The theoretical representation describes the coupling between the solidification and development of density stratification in the liquid in the interior of the cavity. The computed results and experimental observations indicate that for moderate horizontal temperature differences, the vertical stratification can effectively damp convection in the stratified portion of the bulk liquid. Increasing the temperature difference or lateral heat flux across the enclosure sufficiently, initiates formation of a series of horizontal double-diffusive convection layers. The nature of the fluid motion in the bulk is seen to have significant influence on solute redistribution and heat transfer, both at the growth interface and in the interior of the enclosure. The computed flow patterns, solid–liquid interface shapes, and rates of growth of the stratified region compare well with those observed experimentally for directionally-solidified solutions of sodium carbonate and water. The calculated and observed heights of the horizontal convection cells correlate well with theoretical predictions. Order-of-magnitude analysis is used to explore the theoretical limits of stability of the growing layer under the roof with respect to remixing with the underlying 'bulk' liquid.

1. INTRODUCTION

IN THE FOLLOWING we examine the time-dependent physical and chemical evolution of binary double-diffusive solutions crystallizing at a vertical wall. These systems can be divided into two categories: those which preferentially segregate the denser component into the liquid, and those which segregate the lighter component into the liquid.

This work addresses the latter situation, in which compositional and thermal gradients oppose one another, specifically for the parameter range where a complex two-directional or counterbuoyant boundary layer is produced at the crystal interface. The purpose of this study is to develop a mathematical model describing combined convective heat and mass transport during transient solidification, and to validate the theory by comparison with controlled experiments in an aqueous solution.

The current work represents an extension of our previous study of double-diffusive solidifying systems with reinforcing buoyancy effects [1] to the more complicated situation where solutal and thermal effects oppose one another. Together, these papers are the first successful efforts to develop and apply numerical methods to model complex two-dimensional double-diffusive flow phenomena in horizontally-solidified liquids. Previous investigations have been experimental [2–8] or have addressed only the steady-state boundary layer flow at the crystal interface [9–12]. There are no existing theoretical descriptions which include the effects of a moving phase boundary of the time-dependent evolution of the bulk liquid phase within the solidification 'cavity'.

In this paper we use both mathematical and physical modelling to examine the process by which a homogeneous, binary liquid in a square cavity develops vertical, density and compositional stratification and subsequent double-diffusive instabilities owing to the counterbuoyant flow along a vertical or nearly-vertical solidification interface. The experimental measurements are described in Section 2 and the analysis is presented in Section 3. Sections 4 and 5 contain the discussion and the concluding remarks, respectively.

2. SOLIDIFICATION OF AQUEOUS SODIUM CARBONATE SOLUTIONS

The development of density stratification in a 10% liquid due to double-diffusive counterflow is rep-

† Current address: Division 6233, Sandia National Laboratory, Albuquerque, NM 87185, U.S.A.

resented using sodium carbonate and water. For concentrations of greater than approximately 6 wt% sodium carbonate (eutectic composition), the crystalline phase is hydrated sodium carbonate and the solute-enriched liquid adjacent to the crystal front is less dense than the bulk liquid. The horizontal temperature and solute concentration gradients produce a counterbuoyant flow at the solidification front. The motion is upward adjacent to the phase boundary, where the compositional effect on the fluid density dominates, while thermally-dominated downflow occurs in the interior.

The experiments provide semi-quantitative information on the effect of counterbuoyant flow on the vertical density stratification in the liquid and the development of double-diffusive layers. Although the qualitative features of solidification in this aqueous system have been investigated previously [4–6], it has been necessary to refine the experimental apparatus (smaller dimensions and simpler geometry) to allow for quantitative comparison with the numerical calculations presented in the following section.

The enclosure was filled with a homogeneous aqueous sodium carbonate solution, and solidified directionally against the cold wall. The experimental apparatus is shown schematically in Fig. 1. The temperatures of the hot and cold walls of the cavity were maintained at 15 ± 1 and -10 ± 1°C, respectively, by pumping preheated water and/or precooled methanol through copper tubing embedded in the copper sideplates. Neutral-density dye was used to represent the circulation patterns, and the location of the phase boundary and the first front (the horizontal interface between the underlying bulk and overlying stratified liquid regions), were recorded periodically. The entire apparatus was enclosed in 10 cm thick styrofoam insulation to reduce heat loss perpendicular to the flow and to minimize wall effects.

Figure 2 shows the development of a stratified, water-rich zone in the upper portion of the enclosure during the solidification of a 10 wt% sodium carbonate solution. The rate of movement of the solid–liquid interface was rapid during the initial stages ($\sim$0.2 cm min^{-1} for times less than 2 min). Counterflow was initiated within the first 2 min, and within 5 min a region of less dense, fractionated liquid had accumulated in the upper corner adjacent to the crystal front. Within 12 min, this buoyant liquid had reached the far (heated) boundary (Fig. 2(a)), and the maximum convective velocities in the system were estimated at 10–15 (vertical) and 3–5 cm min^{-1} (horizontal).

The ascending liquid from the counterbuoyant flow collected to form a distinct zone above the main thermal convection cell. As solidification progressed, additional liquid accumulated in this zone and the position of the first front migrated downward from the roof (Figs. 2(b) and (c)).

During the first 15 min, most of the liquid in the ascending flow travelled to the top, spreading out above the previously accumulated liquid (Fig. 2(a)) in a manner analogous to the 'box-filling' process described by Baines and Turner [13]. However, as the system evolved (Figs. 2(b) and (c)), only the lightest fluid subject to the strongest upward buoyancy force was able to reach the roof. Fluid further from the crystals, being less enriched in solute, was less buoyant, and was deflected horizontally into the

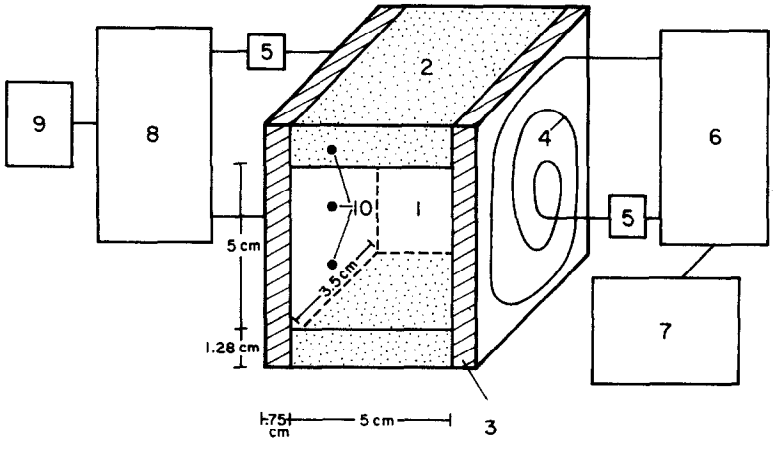

FIG. 1. Schematic diagram of the experimental apparatus used for the study of the solidification behavior of sodium carbonate solutions: 1, plexiglas cavity of inner dimensions $5\times5\times3.5$ cm; 2, 1.28 cm thick plexiglas base and removable lid; 3, 0.75 cm thick copper sidewalls; 4, tubing embedded in sideplates for circulation of coolant; 5, variable flow rate circulation pumps; 6, cold temperature reservoir (methanol); 7, adjustable-temperature refrigeration unit; 8, hot/room temperature reservoir (water); 9, immersion heater; 10, schematic location of thermocouples along vertical walls (also on cold wall).

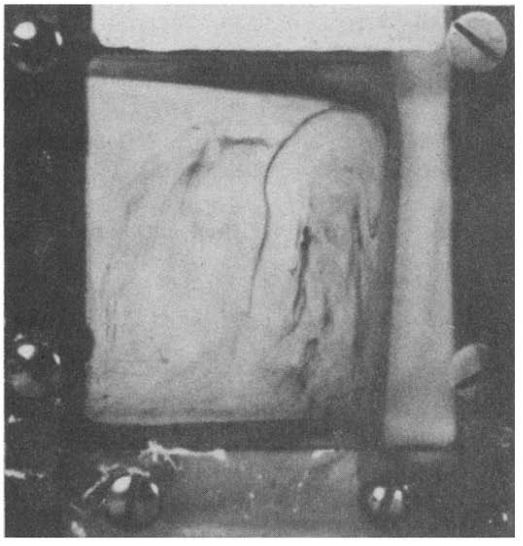

(a)

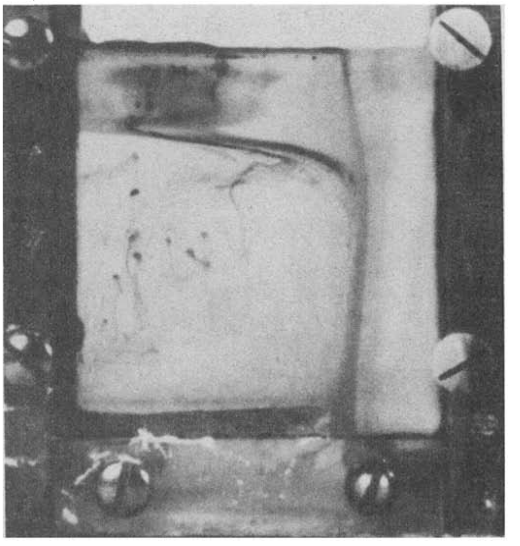

(b)

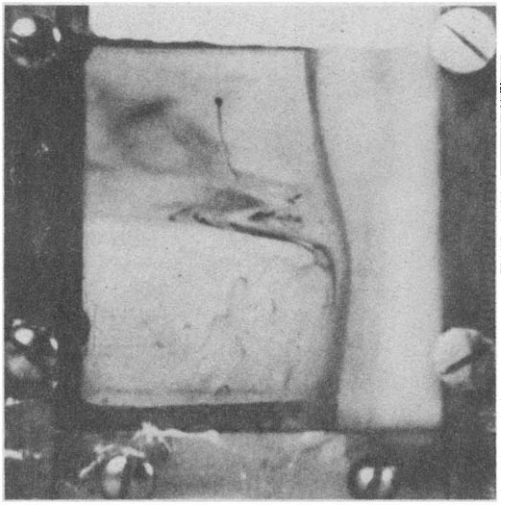

(c)

FIG. 2. Sequence of photographs of the solidification of a solution containing 10 wt% sodium carbonate, illustrating the growth of a water-enriched zone at the top of the cavity. (a) At 12 min, the intrusion of the lighter fluid reaches the heated boundary. (b) At 30 min, the position of the first front is descending from the roof as additional liquid is fed to the upper zone. The fluid from the counterbuoyant boundary layer spills-off horizontally into the stratified zone. (c) At 45 min, the position of the first front is at the midheight of the cavity and the upper layer of lighter liquid is nearly stagnant in comparison to the thermal convection beneath. The 'spill-off' from the boundary layer is concentrated at the level just above the first front.

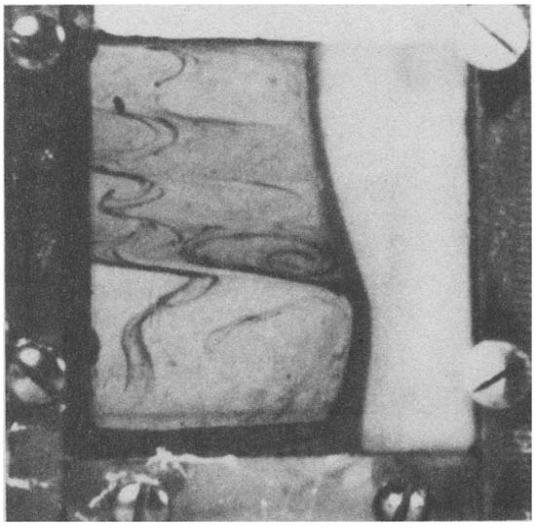

(a)

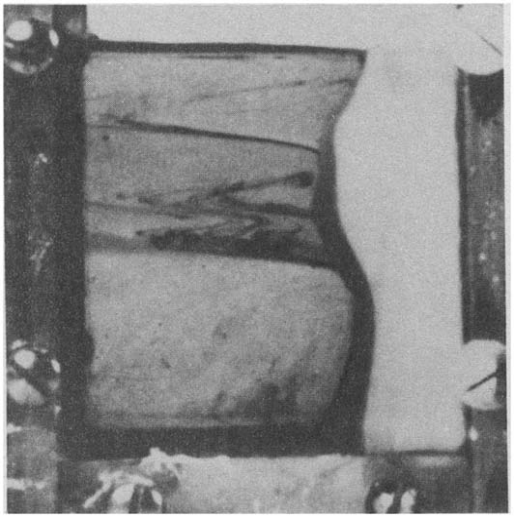

(b)

FIG. 3. Photographs of the same experiment, showing the response of the system to an increase in the temperature of the heated boundary after 45 min. (a) After 4 min, the cellular motion has gained strength, forcing the 'spill-off' channels between the cells to be progressively pinched off. (b) Increasing the temperature further results in increased flow velocities within the cells and partial melting of the solid. The average cell height is increased and only three double-diffusive cells are visible above the the first front.

interior by a 'spill-off' process similar to thermal stratification effects observed elsewhere [14, 15]. The spill-off produced a stable, vertical density and compositional stratification in the fluid above the first front, stabilizing the fluid and damping out the thermal convection in the upper layer. The presence of the stagnant layer is evidenced by the approximately vertical dye streaks in the upper region in Fig. 2(c).

The shape of the solid–melt interface reflects the convective heat transfer patterns. Initially (Fig. 2(a)), thermal convection was dominant and solidification was rapid at the base where the thermal boundary layer was thickest. The onset of counterflow produced a thickening of the boundary layer near the roof also, creating an inwardly concave crystal–melt surface (Fig. 2(c)).

As solidification progressed, fluid continued to accumulate in the upper layer, and the first front descended to the base of the cavity. The vertical extent of the density-stratified region increased at the expense of the underlying thermal convection cell, and fluid motion within the stratified layer became increasingly damped, until the liquid was essentially stagnant.

If, however, the thermal conditions at the heated boundary were altered during solidification, the convective motion within the upper density-graded layer was immediately affected. Figure 3 shows the results of a second experiment, in which the heat input to the heated wall was increased after 45 min of solidification, at the time when the first front had reached the midheight of the cavity. The increased horizontal temperature difference destabilized the stagnant layer, producing four double-diffusive layers (Fig. 3(a)) within the compositionally-zoned liquid with convective velocities of 1–2 cm min^{-1}. The formation of the double-diffusive layers caused the 'spill-off' from the compositional boundary layer to be concentrated into channels along the horizontal surfaces separating adjacent cells (Fig. 3(a)). With continued heating of the wall, convective velocities increased slightly (to 3–5 cm min^{-1}), and the 'spill-off' channels were progressively pinched off. Increasing the temperature of the heated boundary by an additional 5°C decreased the number of double-diffusive cells to three (Fig. 3(b)) and initiated meltback of portions of the solid–liquid boundary.

3. ANALYSIS

In developing a mathematical representation of the system, as a first step, we examine a binary, double-diffusive liquid in an enclosure with stationary walls, and in the second half of this section we incorporate crystallization effects.

The fluid is initially homogeneous in composition and temperature, and is confined to a cavity with the geometry and boundary conditions shown schematically in Fig. 4. A constant solute concentration is specified along the cold wall, while the other boundaries are specified as impermeable.

The density of the binary liquid is given, as a function of solute concentration $\{S'\}$ and temperature $\{\theta'\}$, by a linear equation of state of the form

$$\rho = \rho^0\{1-\beta_T(\theta'-\theta^0)+\beta_S(S'-S^0)\}. \quad (1)$$

The momentum, energy and mass conservation equations for a Boussinesq fluid, expressed in terms of vorticity $\langle\omega\rangle$ and stream function $\langle\Psi\rangle$, are as follows:

$$\frac{1}{\sigma}\frac{D\omega}{Dt} = \nabla^2\omega + (R_T\nabla\theta_x - R_S\nabla S_x) \tag{2}$$

$$\nabla^2\Psi = -\omega \tag{3}$$

$$\frac{D\theta^1}{Dt} = \nabla^2\theta^1 \tag{4}$$

$$\frac{DS}{Dt} = (Le)^{-1}\nabla^2 S \tag{5}$$

where the symbols and operators are defined in Table 1.

The time-dependent problem described by equations (1)–(5) is solved numerically in conjunction with the assumed boundary and initial conditions of Fig. 4, for a binary liquid in which the solute is the lighter component. The solution grid employs 51 uniformly-spaced points in the vertical direction, and 54 non-uniformly spaced points in the horizontal direction. Care was taken to position between 4 and 6 grid points within the estimated width of the concentration boundary layer as defined by the values of Le, R_T. A complete description of the finite difference scheme and the numerical procedure used to solve this system of coupled partial differential equations has been provided elsewhere [1, 16].

In the following, we present a selection of the computed results using the values of the dimensionless quantities listed in Table 2, which correspond to the physical parameters of the aqueous sodium carbonate

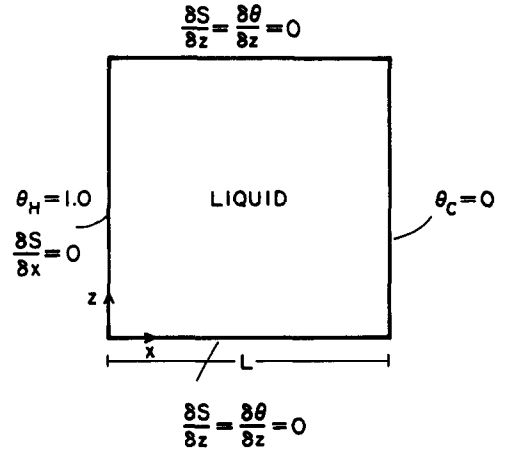

FIG. 4. Schematic illustration of the model system used in the first calculation, assuming planar, stationary vertical boundaries.

Table 1. Symbols and operators (primes denote dimensional quantities)

$t = \frac{t'\kappa}{L^2} = t'/\tau$	dimensionless time
$x = \frac{x'}{X(z,t)}$	dimensionless horizontal distance (liquid)
$x = \frac{(x' - X\{z,t\})}{(L - X\{z,t\})}$	dimensionless horizontal distance (solid)
$z = \frac{z'}{L}$	dimensionless vertical distance
$u = \frac{u'L}{\kappa}$	dimensionless horizontal velocity
$v = \frac{v'h}{\kappa} = v/\zeta$	dimensionless vertical velocity
$\omega = \frac{\omega' L^2}{\kappa}$	dimensionless vorticity
$\Psi = \frac{\Psi'}{\kappa}$	dimensionless stream function
$f = 1 + \left(\frac{\partial\delta}{\partial z}\right)^2$	interface shape factor
$\delta = \frac{X'(t,z)}{L}$	relative width of liquid
$\theta = \left(\frac{T' - T^0}{\Delta T}\right)$	dimensionless temperature
$S = \left(\frac{S' - S^R}{\Delta S}\right)$	dimensionless solute concentration
$X(t)'$	width of liquid region
h	length scale for cell height
L	characteristic cavity dimension
T^0	initial temperature
S^R	reference solute concentration
ΔT	reference temperature drop
ΔS	reference composition change
Θ_H, Θ_C	temperature of hot, cold walls
k_D	distribution coefficient

Definition of operators

$$\frac{D\langle\ \rangle}{Dt} = \frac{\partial\langle\ \rangle}{\partial t} + u\frac{1}{\delta}\left(\frac{\partial\langle\ \rangle}{\partial x}\right) + v\left(\frac{\partial\langle\ \rangle}{\partial z}\right)$$

$$\nabla^2\langle\ \rangle = \frac{1}{\delta^2}\left(\frac{\partial^2\langle\ \rangle}{\partial x^2}\right) + \left(\frac{\partial^2\langle\ \rangle}{\partial z^2}\right) \quad \text{liquid region}$$

$$\nabla^2\langle\ \rangle = \frac{1}{(1-\delta)^2}\left(\frac{\partial^2\langle\ \rangle}{\partial x^2}\right) + \left(\frac{\partial^2\langle\ \rangle}{\partial z^2}\right) \quad \text{solid region}$$

$$\nabla\langle\ \rangle_x = \frac{1}{\delta}\left(\frac{\partial\langle\ \rangle}{\partial x}\right) \quad \text{liquid region}$$

$$\nabla\langle\ \rangle_x = \frac{1}{(1-\delta)}\left(\frac{\partial\langle\ \rangle}{\partial x}\right) \quad \text{solid region}$$

Table 2. Physical constants and dimensionless quantities

	Definition	Value used in calculations
ρ	density	1.0 g cm^{-3} (15 wt% Na_2CO_3) 1.16 g cm^{-3} (0 wt% Na_2CO_3)
κ	thermal diffusivity	1.5×10^{-3} cm^2 s^{-1} (liquid) 1.5×10^{-3} cm^2 s^{-1} (solid)
k	thermal conductivity	1×10^{-3} cal cm^{-1} s^{-1} °C^{-1} (liquid) 1×10^{-3} cal cm^{-1} s^{-1} °C^{-1} (solid)
ΔH	latent heat of fusion	76 cal g^{-1}
ν	kinematic viscosity	0.93×10^{-2} cm^2 s^{-1}
D	solute diffusivity	1.5×10^{-5} cm^2 s^{-1}
β_T	coefficient of thermal expansion	3×10^{-4} °C^{-1}
β_S	coefficient of solutal expansion	8×10^{-3} (wt%)$^{-1}$
m'	slope of liquidus line	1.7°C (wt%)$^{-1}$
k_D	distribution coefficient	0
L	characteristic length (average cell size)	5 cm
h	length scale for secondary cells	0.6–0.7 cm (advanced stage) (intermediate)
$\sigma = \frac{\nu}{\kappa}$	Prandtl number	6
$Le = \frac{\kappa}{D}$	Lewis number	50
$R_T = \frac{g\beta_T \Delta T L^3}{\nu\kappa}$	thermal Rayleigh number	2×10^6
$R_S = \frac{g\beta_S \Delta S L^3}{\nu\kappa}$	solutal Rayleigh number	R_T/Γ
$St = \frac{\Delta H}{C_p \Delta T}$	Stefan number	5.0
$\gamma = \frac{\kappa_l}{\kappa_s}$	ratio of thermal diffusivities of solid and liquid	1.0
$K = \frac{k_l}{k_s}$	ratio of thermal conductivities of solid and liquid	1.0
$\Gamma = \frac{\beta_T \Delta T}{\beta_S \Delta S}$	buoyancy ratio	0.22–0.02
R_c	critical Rayleigh number at onset of instability	1.5×10^4

system. The principal parameters governing the behavior of the system are the Lewis number, the thermal Rayleigh number (calculated using a characteristic length scale equal to either the height of the enclosure (L) or the average height of the double-diffusive walls $\{h\}$), and the relative buoyancy ratio $\{\Gamma\}$. The thermal Rayleigh number appropriate for the experimental system during the early stages (based on L), is estimated to be of the order of 1×10^7–2×10^7, while that based on the average height of the double-diffusive cells is estimated at 1×10^6–2×10^6. Although it has not been practical to extend the calculations to thermal Rayleigh numbers beyond 2×10^6, and Lewis numbers of ~ 50, the computed results are most sensitive to changes in Γ, the value of which can be varied over the complete range of interest for these systems.

The sequence of contour plots for stream function, temperature and solute concentration depicted in Figs. 5–7 illustrate the calculated results for an R_T of 10^6, a relative buoyancy of 0.2, and a Lewis number of 50.

It is seen that within a short time ($t < 1$ min), diffusion of solute away from the cold wall generates a narrow concentration boundary layer, and the lighter, solute-enriched liquid within this boundary layer ascends to the roof of the enclosure where it spreads out horizontally. The lighter liquid remains distinct from the homogeneous liquid beneath it, and collects to form a stable horizontal layer below the roof (Fig. 5(a)). The fluid in the interior of the enclosure develops a vertical solute gradient (Fig. 5(c)) and inverse (relative to the lower region) temperature profile (Fig. 5(b)) under the roof.

The position of the first front moves progressively downward (Fig. 6), and the extent of the density-stratified upper layer increases. The combination of the horizontal temperature gradient (Fig. 6(b)) and the vertical density gradient (Fig. 6(c)) leads to the initiation of horizontal double-diffusive layers in the upper zone.

Figure 7(a) shows well-developed horizontal double-diffusive motions above the first front, and illustrates

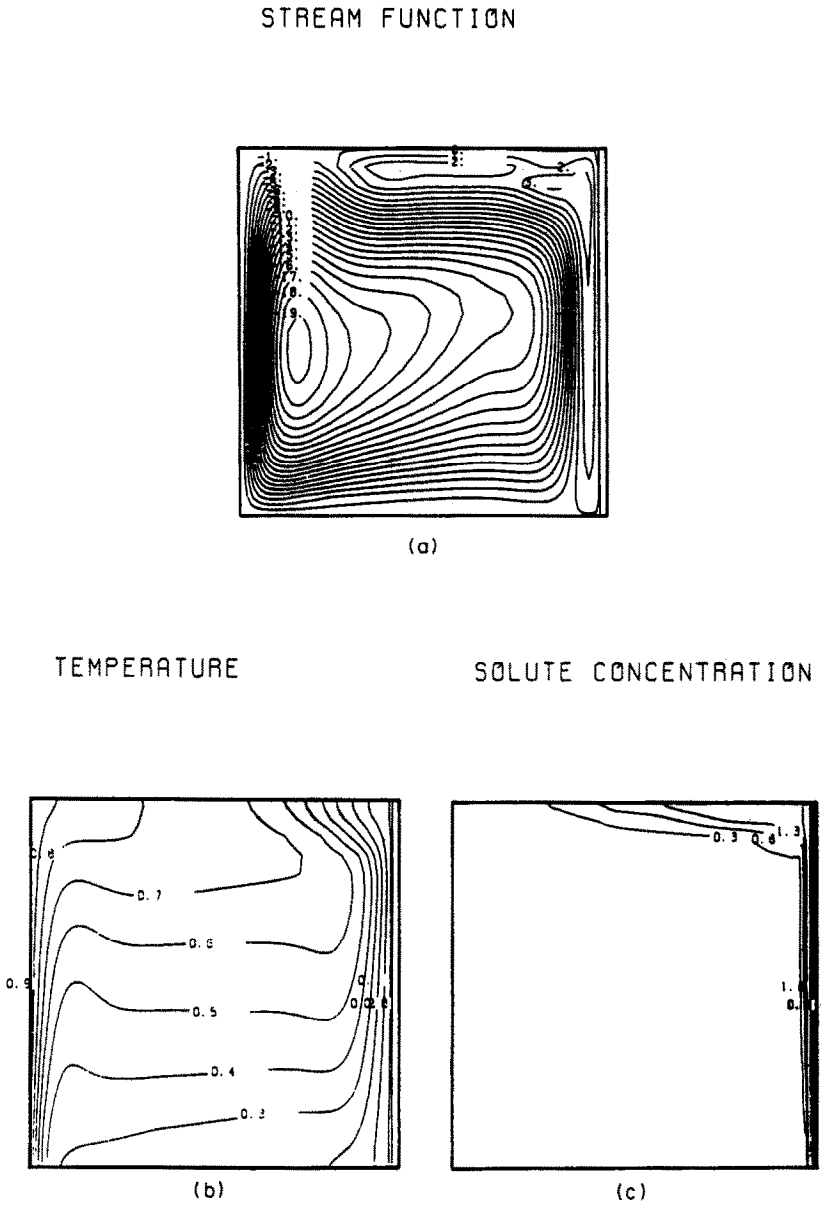

FIG. 5. Contour diagrams of the calculated (a) stream function, (b) temperature and (c) solute concentration after 10.2 min, based on a Lewis number of 50, a thermal Rayleigh number of 1×10^6, and a buoyancy ratio of 0.2. The counterflow transports the cooler, solute-rich liquid from the base of the cavity upward along the right-hand wall and a short distance out above the thermally-convecting, homogeneous liquid.

the manner in which the fluid from the boundary layer 'spills off' into the interior along a channel at the roof and above the first front. The interior of these horizontal cells is well mixed with respect to solute concentration and temperature (Figs. 7(b) and (c)), while the horizontal boundaries in between are characterized by steep vertical gradients.

A comparison of the calculated results with the photographs of Section 2 verifies the ability of the theoretical analysis to reproduce the evolution in flow patterns observed during the solidification experiments. However, the correspondence between the calculations and experiments in terms of time (based on a value of the time constant (τ) of 5×10^3 s) becomes less accurate at large times due to the artificial conditions applied at the cooled wall (stationary, planar, constant composition). The mathematical representation can be improved by including a moving phase boundary to account for the dependence of the mass flux boundary condition on the solidification rate.

A schematic representation of the more complex model is shown in Fig. 8. At time $t = 0$, the temperature of the right-hand wall of the cavity is set at

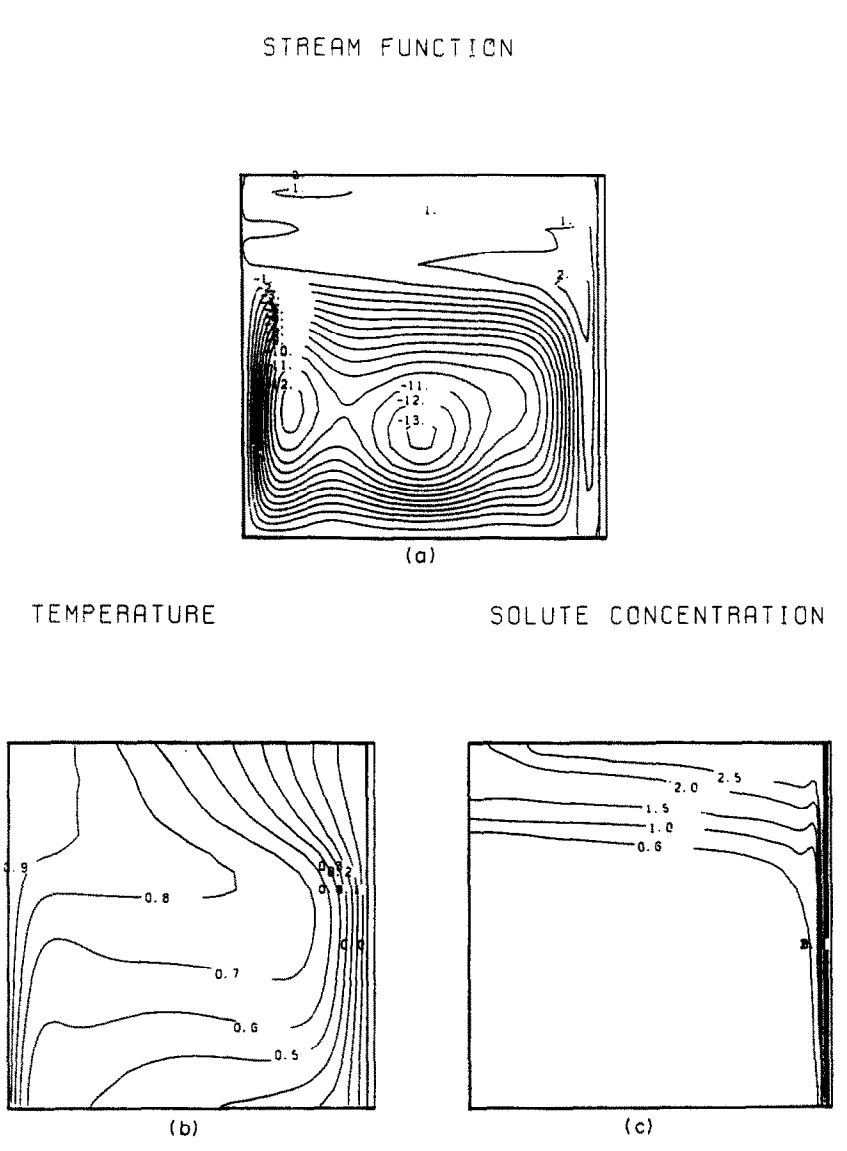

FIG. 6. Same as Fig. 5, calculated at 30.7 min. As additional solute-rich liquid is added to the upper layer, the position of the first front moves downward and the region of stable density and solute stratification expands further into the liquid.

-1.0, and the formation of a solid phase of composition

$$S^s = k_D S^l \tag{6}$$

is initiated. In the solid phase diffusion of the solute is assumed negligible and the conservation of energy requires

$$\frac{\partial \theta^s}{\partial t} = \gamma \nabla^2 \theta^s. \tag{7}$$

The boundary conditions along the outer cavity walls are as shown in Fig. 8, while those along the solid–liquid interface ($x = x(z, t)$) express the conservation of mass and energy according to

$$(K \nabla \theta_x^s - \nabla \theta_x^l) f = St \frac{\partial \delta}{\partial t} \tag{8}$$

$$\nabla S_x f = Le\, S^*(k_D - 1) \frac{\partial \delta}{\partial t} \tag{9}$$

as well as the relationship between the equilibrium melting temperature (θ^*) and solute concentration (S^*)

$$\theta^* = \theta_{mp} + mS^* \tag{10}$$

where θ_{mp} is the melting point of the pure solvent.

To account for the shape of the phase boundary, the governing equations are rewritten according to the Landau boundary immobilization technique [17–23]. At each time step, the liquid and solid regions are transformed into rectangular domains. In transformed space, the horizontal coordinate (x) in the liquid

$$x = \frac{x'}{X(z, t)}$$

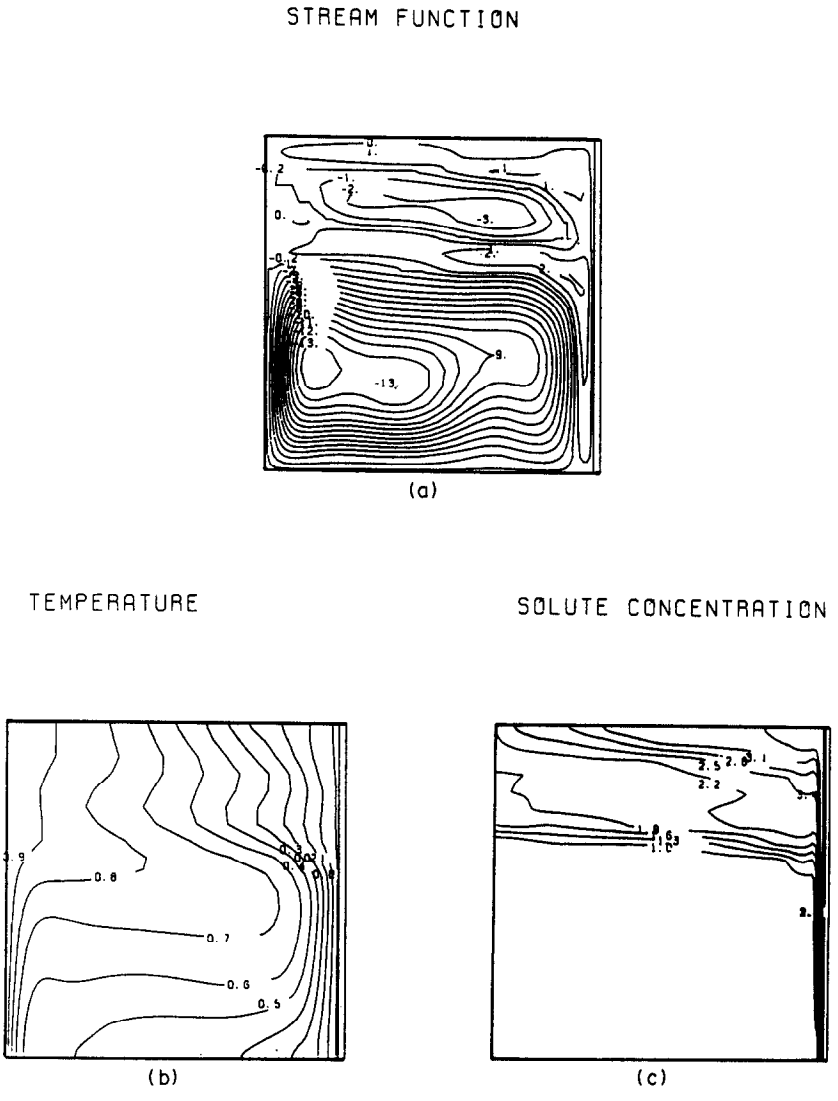

FIG. 7. Same as Fig. 5, calculated at 64.2 min. The upper layer develops horizontal double-diffusive cellular motion, which opposes the counterbuoyant circulation. Channels of 'spill-off' fluid are evident at the roof and above the first front.

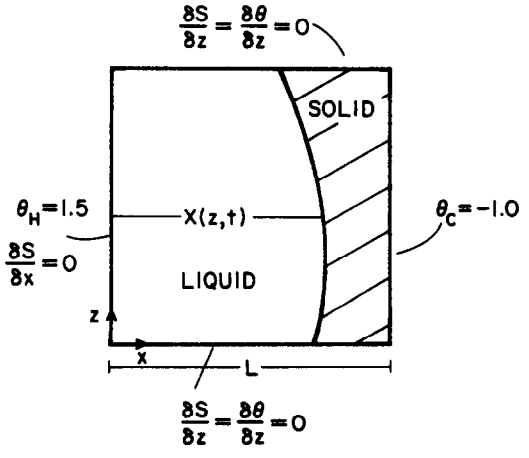

FIG. 8. Schematic diagram of geometry and boundary conditions used in the solidification calculation.

given in terms of the spatial coordinate in physical space $\{x'\}$ and the width of the liquid region $\{X\}$, ranges from 0 to 1 for all z and t. The advantage of this approach is that the solid–liquid boundary in transformed space is stationary, and defined by the position $x = 1$ during any given time interval.

The final form of the governing equations and boundary conditions in the adjusted coordinate system are based on the 'quasi-stationary' approximation. The use of this approximation implies that over a limited time interval, the effect of the interface motion on the temperature, solute and flow fields in the melt is negligible. Sparrow *et al.* [21], Ho and Viskanta [22], Ramachandran *et al.* [19] and Duda *et al.* [23] have demonstrated that the quasi-stationary approximation is valid for most phase change problems with natural convection at moderate and large Stefan numbers.

In addition, our analysis assumes that the thickness of the melt region ($X(z, t)$) varies slowly with z, so that terms involving $\partial X/\partial z$ in the transport equations can be neglected. Ramachandran *et al.* [19] and Ho and Viskanta [22] have shown that this simplification is valid in systems as long as the vertical heat transfer across the upper and/or lower surfaces of the liquid and solid regions is not extreme.

The use of these approximations is believed to be justified because of the magnitude of the Stefan number and the nature of the thermal boundary conditions at the horizontal boundaries.

A grid spacing similar to that described for the previous sequence of calculations is used for the liquid region, while uniform grid spacing is used in both directions in the solid region.

Figures 9 and 10 illustrate the evolution of the circulation patterns, temperature and solute concentration distributions accompanying progressive solidification. The calculations depict the behavior of a system characterized by a Lewis number of 50 and thermal and nominal solutal (R_S) Rayleigh numbers of 2×10^6.

The onset of counterflow and the initial development of the fractionated zone at the roof occurs in much the same manner as in the previous calculations with a stationary cold wall. The maximum calculated velocities in the counterbuoyant boundary layer and the horizontal intrusion layer at the top of the cavity are initially as high as 15 and 4 cm min^{-1}, respectively, in agreement with the velocity estimates derived from the experiments. With continued solidification, the vertical extent of the upper zone increases (Figs. 9(a)–(10a)) and due to this density stratification, the liquid becomes progressively more stagnant.

Within 48 min (Fig. 10), the velocity of the

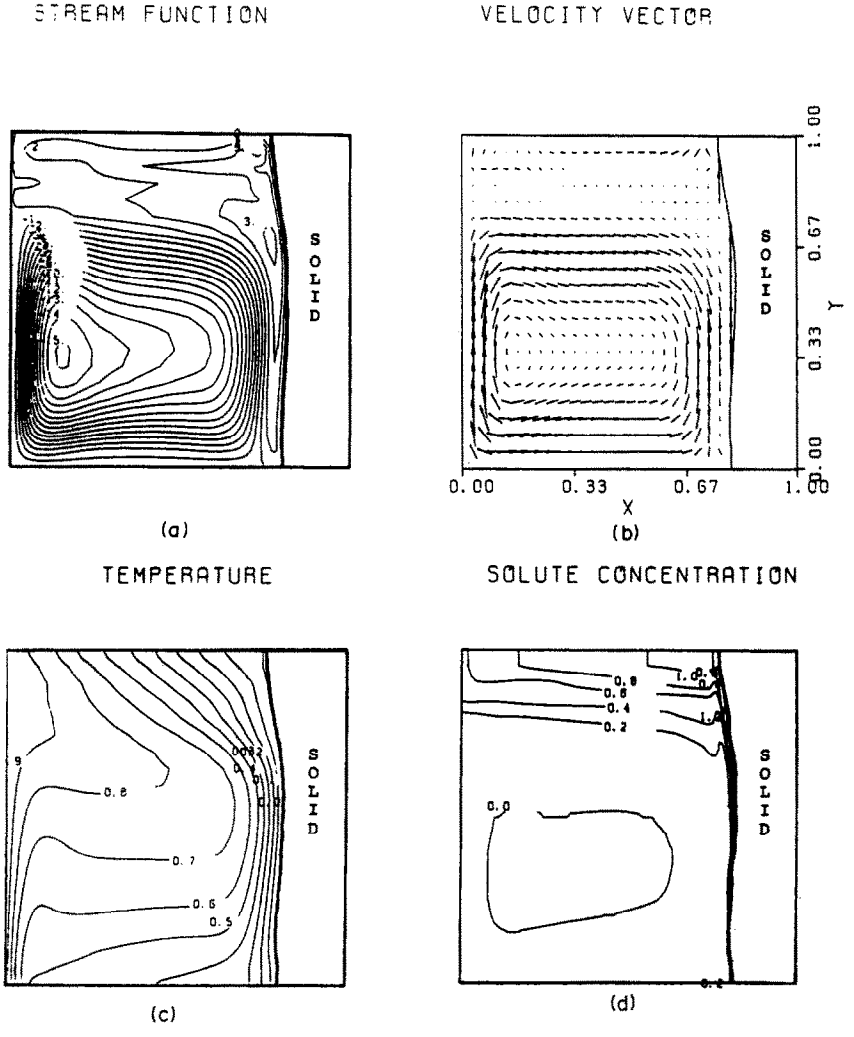

FIG. 9. Computed results of the solidification calculation showing the calculated (a) stream function, (b) velocity vector, (c) temperature, and (d) solute concentration after 34.1 min for a thermal Rayleigh number of 2×10^6 and a Lewis number of 50. Counterflow creates an upper layer of stratified liquid under the roof and causes solidification near the top of the cavity to be rapid, where the thermal boundary layer is thickest.

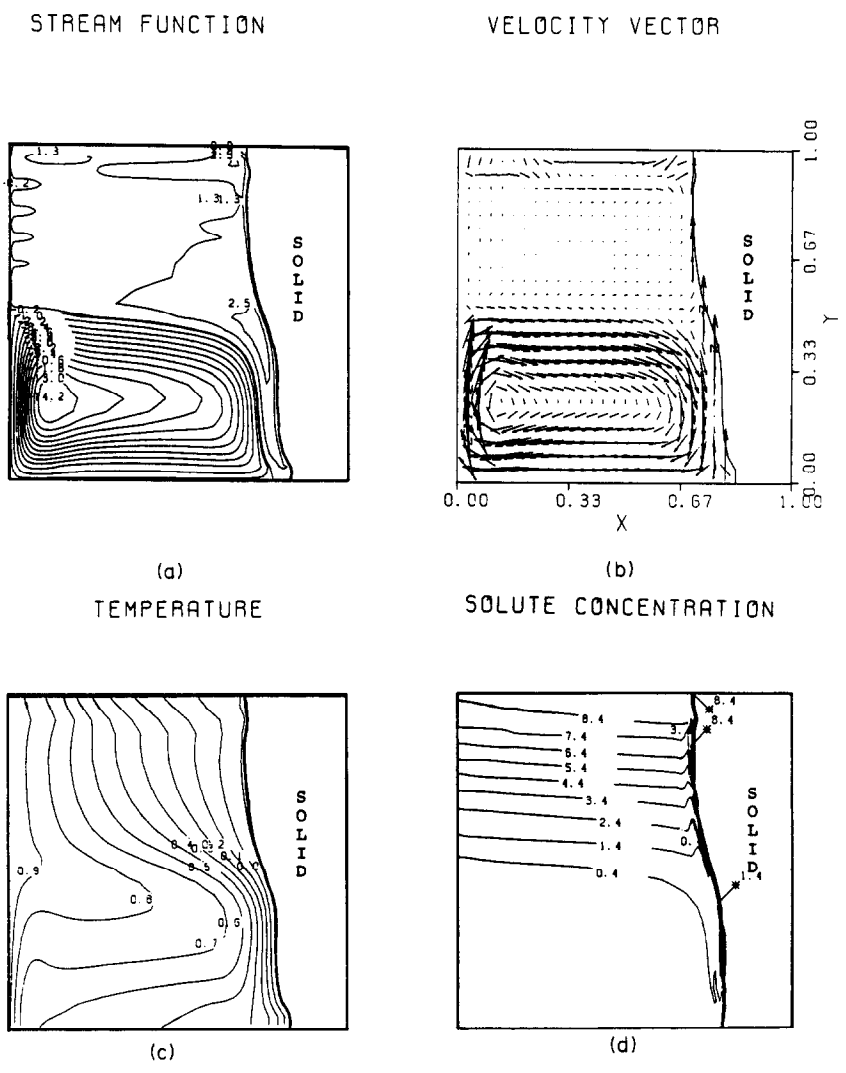

FIG. 10. Same as Fig. 9, but after 47.8 min. The first front has descended to the midheight of the cavity, and the stratification has effectively damped out the thermal convection except for regions where 'spill-off' from the vertical boundary layer is apparent.

counterbuoyant flow has decreased to 5 cm min^{-1} owing to the decreased solidification rate and the establishment of density gradients in the bulk liquid. The boundary layer spills off into the interior of the upper zone (Fig. 10(a)), particularly at the top and base of the upper zone, due to the presence of the solid boundary and the density discontinuity at the first front. Convective mixing within the upper density-stabilized layer is sufficiently reduced so that the vertical solute gradient above the first front is nearly linear (Fig. 10(d)) and the isotherms are approximately vertical (Fig. 10(c)).

Figures 9 and 10 also illustrate the effect of the convective heat transfer pattern in determining the shape of the solid–liquid interface. Due to the inverted thermal gradient above the first front, solidification is more rapid near the top of the enclosure where the counterbuoyant flow is deflected laterally, and transports heat away from the crystallization boundary.

The calculations predict flow patterns and solid–liquid interface shapes consistent with those observed during the first part of the solidification experiment of Section 2. Under those conditions, the magnitude of the horizontal thermal gradient is insufficient to produce any substantial convection within the density-stabilized liquid, and the liquid in the upper zone remains virtually stagnant.

At the time when the position of the first front is approximately at the midheight of the cavity ($t = 48$ min : Fig. 10), the temperature of the heated (left) wall is raised to $\theta = 3$ ($R_T = 6 \times 10^6$), to simulate (approximately) the thermal history of the experiment described in Section 2. The increase in the lateral temperature gradient is sufficient to destabilize the stable solute stratification and cause the formation of two double-diffusive cellular instabilities in the liquid region above the first front. The double-diffusive layers cause the 'spill-off' from the counterbuoyant

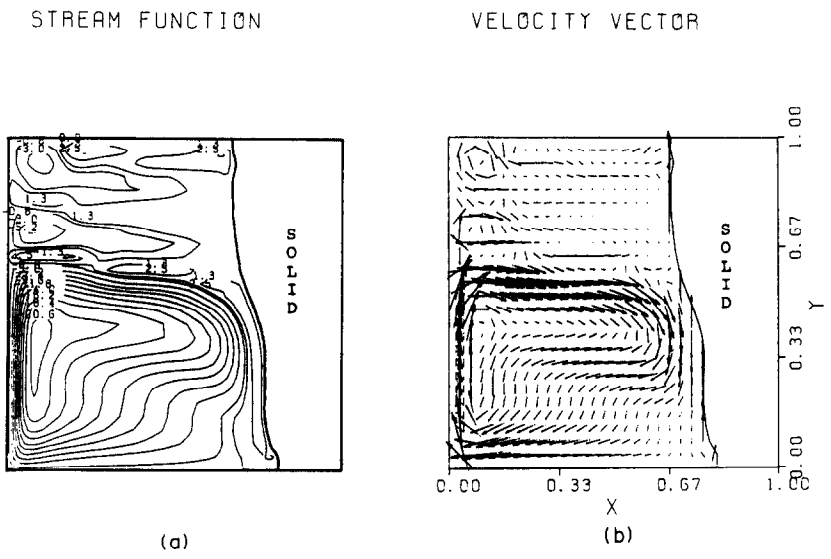

FIG. 11. Same as Fig. 12, but showing the effect of increasing the dimensionless temperature of the heated boundary to 3 (effective thermal Rayleigh number of 6×10^6), on the flow patterns in the liquid after an additional 2 min. The increased temperature gradient initiates double-diffusive instabilities at the heated wall in the (previously) stagnant stratified liquid above the first front.

layer to be concentrated into horizontal channels between the cells. The horizontal layers rapidly gain momentum and propagate towards the solid–liquid boundary (Fig. 11(a)). The increased heat input and corresponding decrease in solidification rate cause the volume and momentum of counterbuoyant flow along the crystal front to decrease. As a result, the 'spill-off' channels become progressively pinched off (Figs. 11(a) and 12(a)). The establishment of the double-diffusive layers above the first front perturbs the isotherms (Fig. 12(c)) and produces a layered solute concentration distribution within the upper zone (Fig. 12(d)), analogous to patterns typically associated with thermohaline layered convection.

4. DISCUSSION

The establishment of a stably-stratified layer of fluid under the roof depends on the ability to generate and sustain a double-diffusive counterbuoyant flow of sufficient momentum to transport fractionated liquid produced by crystallization to the upper region of the cavity. Nilson [10], Nilson *et al.* [11] and Spera *et al.* [12] analyzed double-diffusive boundary layers for steady-state conditions at a stationary wall in an infinite, homogeneous fluid, and determined that counterbuoyant flow is favored by a low Lewis number and a strong solutal buoyancy influence (small Γ). The aqueous sodium carbonate solutions are characterized by Lewis numbers of ~ 100 and buoyancy ratios of ~ 0.15, and therefore fall well within the limits of the counterflow region. In contrast, metallic systems are characterized by relatively high Lewis numbers, and counterflow is only possible for very high solutal buoyancy effects ($\Gamma < 0.11$ for $Le = 10^3$, and $\Gamma = 0.017$ for $Le = 10^5$).

However, there is evidence that metallic liquids become stratified during solidification in a manner similar to that described in aqueous solutions [24–29]. One explanation is that metallic systems solidify with a non-planar interface and, as a result, solute segregation occurs across the two-phase region, creating a wider 'effective' concentration boundary layer (δ_c). Increasing the boundary layer thickness has essentially the same effect on the stability of counterflow as increasing the solutal buoyancy force or decreasing the Lewis number. Therefore, the presence of a two-phase region may actually promote the onset of counterflow in metallic systems. Preliminary calculations based on the physical parameters of the Pb–Sn system ($Le \sim 8 \times 10^2$) are in agreement with the experimental observations of Fisher and Hunt [28] and Hebditch and Hunt [26], and predict the development of stable solute stratification as a result of unidirectional boundary layer flow in an Sn-rich alloy and counterflow in a Pb-rich alloy.

In double-diffusive counterbuoyant situations, the rate at which fractionated fluid accumulates determines the importance of the stratification process, and therefore influences the solute distribution in both liquid and solid phases. If the counterflow is weak, the stratification has only a minor effect on solute redistribution in the system, whereas when accumulation rates are high, the vertical solute gradient develops rapidly, and counterflow will have a determining influence on the spatial and temporal variations in the composition of the liquid and solid phases.

The accumulation rate is measured in terms of the 'volumetric' flow rate (M) of fluid in the concentration

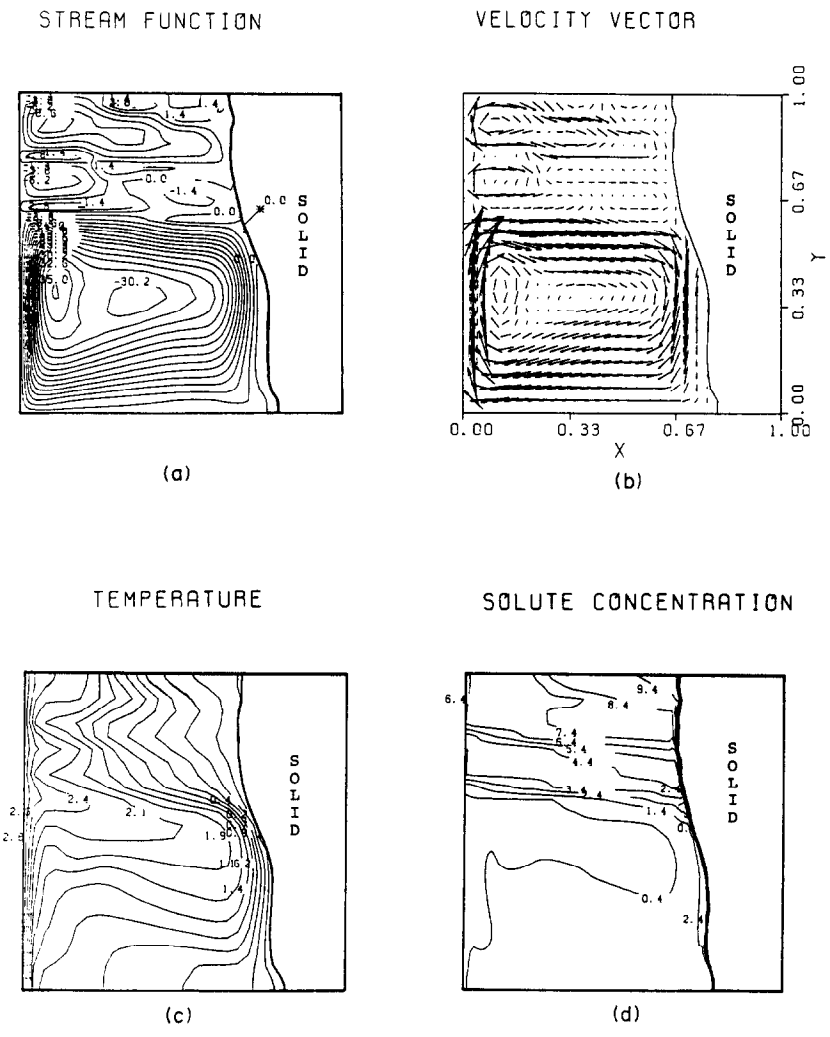

FIG. 12. Same as Fig. 11, but after 5 min. The cells are well established above the first front, and the 'spill-off' is almost totally pinched off. The isotherms are deformed into a cellular pattern, and the solute distribution has a vertically layered appearance.

boundary layer (δ_c) past an elevation z†

$$M \propto \int_0^{\delta_c} v(x, z)\, dx \sim \delta_c V_c \tag{11}$$

evaluated at an appropriate height along the vertical boundary (M_{max} at $z \sim L$). The orders of magnitude of V_c, δ_c are given as functions of R_S

$$V_c \sim \frac{(R_S D\kappa)^{1/2}}{L} \tag{12}$$

$$\delta_c \sim \frac{L}{Le^{1/4} R_S^{1/4}} \tag{13}$$

leading to an estimated accumulation rate of

$$M \sim R_S^{1/4} \kappa^{1/4} D^{3/4}. \tag{14}$$

† Due to the two-dimensional nature of the system, the dimensions of M will be cm^2 s^{-1}.

The boundary layer analysis of Spera *et al.* [12] yields a more exact expression for M, with the same functional dependence on R_S, D and κ.

In Fig. 13, the amount (cm^2) of liquid accumulated in the upper layer is plotted as a function of the time elapsed since the beginning of solidification. The theoretical predictions compare favorably with the measured accumulation rate. During the initial stages, solidification is rapid and the mass flux of lighter solute into the boundary layer is high, producing strong counterflow and rapid accumulation.

The solidification rate decreases with time, causing a decrease in the solutal mass flux at the crystal front. Consequently, the volumetric flow rate in the counterbuoyant boundary layer is lowered, producing the gradual decrease in slope of the experimental and calculated accumulation rate curves shown in Fig. 13. The accumulation and solidification rates exhibit a similar time-dependent behavior, so that the volume of liquid accumulated above the first front increases

roughly proportionately to the volume of solidified material formed.

The order-of-magnitude analysis predicts an accumulation rate of 22 $cm^2\ h^{-1}$ for the experimental system, based on an estimated average $\Delta S = 4$ wt% and corresponding effective $R_S = 2.8 \times 10^8$. The line representing this estimate of the accumulation rate (Fig. 13) falls within the limits of the measured data for the intermediate stages of solidification. This suggests that the order-of-magnitude analysis can be used to estimate the average accumulation rate for a specific system. However, extrapolation of the initial or average accumulation rate results in overestimation of the volume of liquid accumulated in the stratified zone. The numerical simulation, on the other hand, explicitly incorporates the dependence of the solute boundary condition on the solidification rate, therefore providing more accurate information on the time-dependent stratification process. In addition, the analysis presented here accounts for the effect of the continuously evolving solute stratification in the interior as well as the changing aspect of the liquid region.

The counterflow and accumulation processes produce a region above the first front which is characterized by a stable, vertical solute gradient. If this vertical density–solute gradient is sufficiently large in comparison to the horizontal temperature gradient, the upper layer is stabilized and convection within it is effectively damped. However, if the lateral thermal gradient is increased, the density stratification is partly destabilized and a series of horizontal convection layers analogous to thermohaline double-diffusive layers form simultaneously throughout the depth of the stratified layer.

The characteristics of the double-diffusive layers observed in the crystallizing aqueous solutions are similar to the behavior of a linearly-stratified salt solution which is heated or cooled from the side [30]. The distance (l) a fluid element rises to become neutrally buoyant can be related to the average height of the double-diffusive convection layers (h) observed in the experiments according to [30–34]

$$h = c \cdot l = c \cdot \frac{\beta_T \Delta T}{\beta_S \, \mathrm{d}S/\mathrm{d}z}; \quad 0.65 < C < 0.9. \quad (15)$$

In this system $\mathrm{d}S/\mathrm{d}z$ is best defined in terms of the average vertical composition gradient within the upper layer at the time when the temperature of the heated wall is raised. We approximate this as

$$\frac{\mathrm{d}S}{\mathrm{d}z} = \frac{\{S(z = L) - S(z = Z)\}}{\Delta Z} \quad (16)$$

where ΔZ is the depth of the upper layer; z the elevation of the first front; $S(z = Z)$ the initial liquid composition (10 wt% solute); and $S(z = L)$ is the same as at the crystal–liquid interface (6 wt% solute).

When the temperature of the left-hand wall was increased, the upper layer had an average depth of 2.5 cm, suggesting a maximum estimate of $\mathrm{d}S/\mathrm{d}z$ of 1.6 wt% cm^{-1}. The horizontal temperature difference was 30°C, which leads to a predicted value of the vertical length scale $l_{\min} \sim 0.7$ cm, and of the cell height $0.45 < h_{\min} < 0.62$ cm. The observed cell height was ~ 0.6 cm, which is in general agreement with the above approximate analysis.

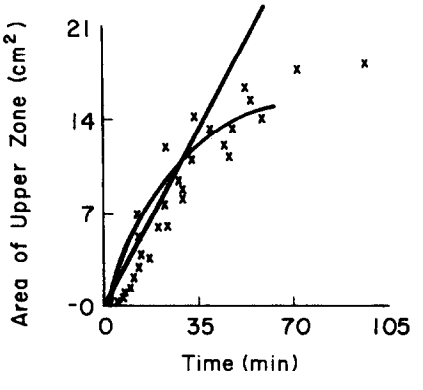

FIG. 13. Plot of area of accumulated liquid above the first front as a function of time. The straight line represents constant accumulation based on the results of the order of magnitude estimate of equation (22), the curves represent the solidification calculation of 3, and the points are selected results of the solidification experiments from 2.

5. CONCLUSIONS

The primary result of this study has been the successful prediction of two-dimensional, transient energy, mass and momentum transfer for a binary double-diffusive liquid with competing thermal and solutal density gradients at a vertical crystal front. The model produces an accurate representation of the behavior observed in aqueous solutions, and our preliminary calculations indicate that it is adequate for studying certain features of metallic alloy solidification. The calculations predict the observed behavior, not only in terms of the double-diffusive counterbuoyant flow at an irregularly-shaped solid interface, but also the interaction between the boundary layer motion and the time-dependent stratification in the interior. Comparison of calculations and experiments indicate the model is time accurate for short- as well as long-time scale phenomena, making it possible to predict the unsteady development of double-diffusive layers in response to transient thermal conditions at the wall. This flexibility will be extremely important when extending the model to crystal growth applications where unsteady thermal conditions may control impurity segregation into the solid.

We conclude that horizontal solidification in double-diffusive systems can transform an initially homogeneous volume of liquid into one exhibiting a pronounced vertical solute and density stratification. In the case of a binary liquid with a lighter solute, the

mechanism for achieving this liquid phase stratification is counterbuoyant flow in a vertical boundary layer along the moving crystal–liquid interface, or by interdendritic flow within a two-phase region. The development of the vertical density stratification in the interior of the cavity acts to stabilize the liquid against thermal natural convection, and leads to the establishment of either stagnant regions in the liquid, or horizontal double-diffusive convecting layers.

REFERENCES

1. M. E. Thompson and J. Szekely, Mathematical and physical modelling of double-diffusive convection in aqueous solutions crystallizing at a vertical wall, *J. Fluid Mech.* **187,** 409–433 (1988).
2. C. F. Chen and J. S. Turner, Crystallization in a double-diffusive system, *J. Geophys. Res.* **85,** 2573–2593 (1980).
3. H. E. Huppert and J. S. Turner, Ice blocks melting into a salinity gradient, *J. Fluid Mech.* **100,** 367–384 (1980).
4. A. R. McBirney, Mixing and unmixing of magmas, *J. Volcan. Geoth. Res.* **7,** 357–371 (1980).
5. A. R. McBirney, B. Baker and R. H. Nilson, Liquid fractionation, Part I: basic principles and experimental simulations, *J. Volcan. Geoth. Res.* **24,** 1–24 (1985).
6. J. S. Turner and L. B. Gustafson, Fluid motions and compositional gradients produced by crystallization or melting at vertical boundaries, *J. Volcan. Geoth. Res.* **11,** 93–125 (1981).
7. E. G. Josberger and S. Martin, A laboratory and theoretical study of the boundary layer adjacent to a vertical melting ice wall in salt water, *J. Fluid Mech.* **111,** 439–473 (1981).
8. V. P. Carey and B. Gebhart, Transport near a vertical ice surface melting in saline water: experiments at low salinities, *J. Fluid Mech.* **117,** 403–423 (1982).
9. V. P. Carey and B. Gebhart, Transport near a vertical ice surface melting in saline water: some numerical calculations, *J. Fluid Mech.* **117,** 379–402 (1982).
10. R. H. Nilson, Countercurrent convection in a double-diffusive boundary layer, *J. Fluid Mech.* **160,** 181–210 (1985).
11. R. H. Nilson, A. R. McBirney and B. Baker, Liquid fractionation, Part II: fluid dynamics and quantitative implications for magmatic systems, *J. Volcan. Geoth. Res.* **24,** 25–54 (1985).
12. F. J. Spera, D. A. Yuen and D. V. Kemp, Mass transfer rates along vertical walls in magma chambers and marginal upwelling, *Nature* **310,** 764–767 (1984).
13. W. D. Baines and J. S. Turner, Turbulent buoyant convection from a source in a confined region, *J. Fluid Mech.* **37,** 51–80 (1969).
14. R. G. Schwind and G. C. Vliet, Observations and interpretations of natural convection in vessels, *Proc. Heat Transfer and Fluid Mech. Inst.*, pp. 51–67. Stanford University Press, Stanford, California (1964).
15. G. Worster and A. M. Leitch, Laminar free convection in confined regions, *J. Fluid Mech.* **156,** 301–319 (1985).
16. M. E. Thompson, Double-diffusive phenomena in horizontally-solidified binary liquids, Ph.D. Thesis, Department of Materials Science and Engineering, M.I.T. (1986).
17. T. Saitoh, Numerical method for multidimensional freezing problems in arbitrary domains, *ASME J. Heat Transfer* **100**(2), 294–299 (1978).
18. C. F. Hsu, E. M. Sparrow and S. V. Patankar, Numerical solution of moving boundary problems by boundary immobilization and a control-volume-based finite difference scheme, *Int. J. Heat Mass Transfer* **24,** 1335–1343 (1981).
19. N. Ramachandran, J. P. Gupta and Y. Jaluria, Two-dimensional solidification with natural convection in the melt and convective and radiative boundary conditions, *Numer. Heat Transfer* **4,** 469–484 (1981).
20. A. Gadgil and D. Gobin, Analysis of two-dimensional melting in rectangular enclosures in the presence of convection, *Trans. ASME* **106,** 20–26 (1984).
21. E. M. Sparrow, S. V. Patankar and S. Ramadhyani, Analysis of melting in the presence of natural convection in the melt region, *Trans. ASME* **99,** 520–526 (1977).
22. C. J. Ho and R. Viskanta, Heat transfer during melting from an isothermal vertical wall, *ASME J. Heat Transfer* **106,** 12–19 (1984).
23. J. L. Duda, M. F. Malone, R. H. Notter and J. S. Vrentas, Analysis of two-dimensional diffusion controlled moving boundary problems, *Int. J. Heat Mass Transfer* **18,** 901–910 (1975).
24. S. M. Copley, A. F. Giamei, S. M. Johnson and M. F. Hornbecker, The origin of freckles in unidirectionally solidified castings, *Metall. Trans.* **1,** 2193–2204 (1970).
25. N. Streat and T. Weinberg, Macrosegregation during solidification resulting from density differences in the liquid, *Metall. Trans.* **5B,** 2539–2548 (1974).
26. D. J. Hebditch and J. D. Hunt, Observations of ingot macrosegregation on model systems, *Metall. Trans.* **5A,** 1557–1564 (1974).
27. R. J. McDonald and J. D. Hunt, Fluid motions through the partially solid regions of a casting and its importance in understanding A-type segregation, *Trans. TMS–AIME* **245,** 1994–1997 (1969).
28. K. M. Fisher and J. D. Hunt, Observations on the nature and extent of gravitational interdendritic fluid flow. *Sheffield International Conference on Solidification and Casting*, Metals Society Book, Vol. 193, pp. 325–330 (1979).
29. R. Mehrabian, M. Keane and M. C. Flemings, Interdendritic fluid flow and macrosegregation: influence of gravity, *Metall. Trans.* **1,** 1209–1220 (1970).
30. C. F. Chen, Onset of cellular convection in a salinity gradient due to a lateral temperature gradient, *J. Fluid Mech.* **63,** 563–576 (1974).
31. C. F. Chen, D. G. Briggs and R. A. Wirtz, Stability of thermal convection in a salinity gradient due to lateral heating, *Int. J. Heat Mass Transfer* **14,** 57–65 (1971).
32. S. A. Thorpe, P. K. Hutt and R. Soulsby, The effect of horizontal gradients on thermohaline convection, *J. Fluid Mech.* **38,** 375–400 (1969).
33. R. A. Wirtz, D. G. Briggs and C. F. Chen, Physical and numerical experiments on layered convection in a density-stratified fluid, *Geophys. Fluid Dynam.* **3,** 265–288 (1972).
34. J. S. Turner, *Buoyancy Effects in Fluids*. Cambridge University Press, London (1979).

STRATIFICATION EN DENSITE DUE A L'ECOULEMENT OPPOSE AU FLOTTEMENT LE LONG D'UN FRONT VERTICAL DE CRISTALLISATION

Résumé—Une modélisation théorique et une expérimentation sont utilisées pour analyser la solidification horizontale d'un liquide binaire dans une cavité fermée rectangulaire. Pour des solutions qui dispersent le composant le plus léger dans le liquide, les gradients de composition et de température, produits pendant la solidification, conduisent à l'apparition d'un écoulement vertical qui s'oppose au flottement le long des cristaux en formation. Ce contre-courant transforme progressivement le liquide initialement homogène en une couche fluide stratifiée, caractérisée par des gradients verticaux prononcés de concentration. La représentation théorique décrit le couplage entre la solidification et le développement de la stratification dans le liquide, à l'intérieur de la cavité. Les configurations d'écoulement, les formes de l'interface solide–liquide, les vitesses de croissance de la région stratifiée se comparent bien avec ce qui est observé expérimentalement pour des solutions de carbonate de sodium et d'eau. Les hauteurs calculées et observées des cellules de convection horizontales s'accordent bien avec les précisions théoriques. L'analyse d'ordre de grandeur est utilisée pour explorer les limites théoriques de stabilité de la couche croissante sous le plafond, en relation avec le remélange du coeur liquide qui est au dessous.

DICHTESCHICHTUNG DURCH ABWÄRTSSTRÖMUNG ENTLANG EINER VERTIKALEN KRISTALLISATIONSFRONT

Zusammenfassung—Mit Hilfe theoretischer Simulation und Experimenten wird die horizontale Erstarrung in einem Zweistoffgemisch unter Berücksichtigung von Diffusionsvorgängen durch Wärme- und Konzentrationsgradienten in rechteckigen geschlossenen Hohlräumen untersucht. Lösungen, bei denen die leichtere Komponente in die Flüssigkeit abgeschieden wird (durch Kristallisation) führen zur Bildung von Konzentrations- und Temperaturgradienten und damit zum Einsetzen einer Abtriebsströmung entlang der wachsenden Kristalle. Diese Strömung ruft in der ursprünglich homogenen Flüssigkeit eine Dichteschichtung hervor, die durch ausgeprägte vertikale Lösungsgradienten gekennzeichnet ist. Die theoretische Untersuchung beschreibt den Zusammenhang zwischen Verfestigung und Entwicklung der Dichteschichtung im Innern des Hohlraums. Die Rechenergebnisse und die Beobachtungen der Experimente ergeben, daß für mäßige horizontale Temperaturunterschiede die vertikale Schichtung die Konvektion in der Flüssigkeit dämpfen kann. Eine Erhöhung der Temperaturunterschiede oder des seitlichen Wärmestroms durch den Hohlraum bewirkt die Bildung einer Reihe von horizontalen Konvektionsschichten. Die Art der Flüssigkeitsbewegung hat dabei einen großen Einfluß auf die Lösungsverteilung und den Wärmetransport, sowohl an den Wachstumsgrenzen als auch im Innern des Hohlraums. Die berechneten Strömungseigenschaften, die Formen der fest-flüssig Grenzschicht und die Wachstumsraten der geschichteten Region stimmen gut mit Beobachtungen an direkt-verfestigten, wäßrigen Natriumkarbonat-Lösungen überein. Auch die Dicke der Konvektionszellen stimmt gut mit der Berechnung überein. Eine Abschätzung der Größenordnung dient zur Bestimmung der theoretischen Stabilitätsgrenze der wachsenden Schicht und deren Vermischung mit der restlichen Flüssigkeit.

СТРАТИФИКАЦИЯ ПЛОТНОСТИ ЖИДКОСТИ, ВЫЗВАННАЯ НАПРАВЛЕННЫМ ПРОТИВ ПОДЪЕМНОЙ СИЛЫ ТЕЧЕНИЕМ У ВЕРТИКАЛЬНОГО ФРОНТА КРИСТАЛЛИЗАЦИИ

Аннотация—Теоретически и экспериментально анализируется процесс горизонтального затвердевания бинарных растворов с взаимной диффузией компонентов в ограниченной прямоугольной полости. Для растворов, в которых происходит сегрегация более легкого компонента, возникают градиенты концентрации и температуры, которые вызывают течение вдоль растущих кристаллов, направленное против действия подъенной силы. Противоток постепенно преобразует первоначально однородную жидкость в слой стратифицированной по плотности жидкости, характеризуемый выраженными вертикальными градиентами концентрации растворенного вещества. Теоретическая модель описывает связь между затвердеванием и стратификацией жидкости по плотности в полости. Результаты расчетов и экспериментальные наблюдения показывают, что при умеренных горизонтальных разностях температур вертикальная стратификация может эффективно подавлять конвекцию в стрифицированном объеме жидкости. При увеличении разности температур или поперечного теплового потока в камере начинается образование ряда горизонтальных конвективных слоев с взаимной диффузией. Очевидно, что характер движения жидкости в объеме оказывает значительное влияние на перераспределение растренного вещества и теплоперенос как на межфазной границе роста кристалла, так и внутри полости. Рассчитанные режимы течения, пормы поверхности раздела между твердым телом и жидкостью и интенсивности роста стратифицированной области хорошо согласуются с экспериментально полученными значениями для направленоо затердевающих растворов карбоната натрия в воде. Рассчитанные и измеренные значения высоты ячеек горизонтальной конвекции хорошо согласуются с теоретически полученными данными. Для определения теоретических пределов устойчивости растущего в закрытом объеме слоя относительно повторного смешения с нижележащим слоем жидкости применяется анализ порядка величин.